

A Bayesian inference method to estimate transmission trees with multiple introductions; applied to SARS-CoV-2 in Dutch mink farms

Bastiaan R. Van der Roest^{a,1}, Martin C.J. Bootsma^{a,b}, Egil A.J. Fischer^c, Don Klinkenberg^d, and Mirjam E.E. Kretzschmar^a

^aJulius Center for Health Sciences and Primary Care, University Medical Center Utrecht, Utrecht University, P.O. Box 85500, Utrecht, Netherlands

^bDepartment of Mathematics, Faculty of Science, Utrecht University, Utrecht, Netherlands

^cDepartment of Population Health Sciences, Faculty of Veterinary Medicine, Utrecht University, Utrecht, Netherlands

^dNational Institute for Public Health and the Environment (RIVM), Bilthoven, Netherlands

Knowledge of who infected whom during an outbreak of an infectious disease is important to determine risk factors for transmission and to design effective control measures. Both whole-genome sequencing of pathogens and epidemiological data provide useful information about the transmission events and underlying processes. Existing models to infer transmission trees usually assume that the pathogen is introduced only once from outside into the population of interest. However, this is not always true. For instance, SARS-CoV-2 is suggested to be introduced multiple times in mink farms in the Netherlands from the SARS-CoV-2 pandemic among humans. Here, we developed a Bayesian inference method combining whole-genome sequencing data and epidemiological data, allowing for multiple introductions of the pathogen in the population. Our method does not a priori split the outbreak into multiple phylogenetic clusters, nor does it break the dependency between the processes of mutation, within-host dynamics, transmission, and observation. We implemented our method as an additional feature in the R-package *phybreak*. On simulated data, our method identifies the number of introductions with high accuracy. Moreover, when a single introduction was simulated, our method produces similar estimates of parameters and transmission trees as the existing package. When applied to data from a SARS-CoV-2 outbreak in Dutch mink farms, the method provides strong evidence for 13 introductions, which is 20 percent of all infected farms. Using the new feature of the *phybreak* package, transmission routes of a more complex class of infectious disease outbreaks can be inferred which will aid infection control in future outbreaks.

Infectious disease outbreak | Transmission tree | Phylogenetic tree | Bayesian inference | Multiple introductions

Correspondence: b.r.vanderroest-2@umcutrecht.nl

31 Introduction

32 Knowledge of who infected whom during an infectious disease outbreak is an important source of information.
33 Characteristics of the outbreak, such as the generation time distribution, are derived from data on these transmission
34 events [31]. Moreover, risk factors for transmission, such as distance between individuals or time lag since infection,
35 can be more accurately quantified, if the infection chain is known. Several methods exist that use data on the time
36 of symptom onset, contacts, or other proximity information, to reconstruct the most likely transmission links between
37 cases [13, 4, 3]. Currently, genetic data is increasingly incorporated into epidemiological inference as an additional
38 source of information to infer individual transmission events, transmission clusters, and even complete transmission
39 trees [9, 12, 22, 27, 29]. The use of both genetic data (i.e., differences in nucleotides between different samples of
40 the pathogen) and epidemiological data (e.g., time of sampling, contacts, and geographic distance) increases the
41 evidence on who infected whom. Moreover, high-risk contacts and superspreaders can be identified when a model
42 is based on both types of data [16, 15]. Therefore, several statistical methods have been developed which take both
43 transmission and evolutionary dynamics of the pathogen into account [5, 23, 30, 10].

44 Most methods assume a single introduction to the population of interest. However, there are many outbreaks where
45 this assumption does not hold, e.g., *Staphylococcus aureus* or *Pseudomonas aeruginosa* are often introduced
46 multiple times on a hospital ward when infected patients are admitted [25], highly pathogenic avian influenza (HPAI)
47 outbreaks among farms are initiated multiple times by wild birds [28], and Foot and Mouth Disease (FMD) can be
48 introduced multiple times from outside a district [17]. Control measures focusing on transmission between hosts may
49 be less effective if there are also external introductions.

50 Currently, several methods to infer transmission trees from both genetic and epidemiological data are available. A
51 method designed by Worby et al. [29] allows for multiple introductions, but it only has phenomenological distributions
52 of genetic distances. There is no underlying mechanistic mutation model for the genetic difference within and
53 between transmission trees. The *outbreaker2* package in R [14] also allows for multiple introductions, but there
54 is only a phenomenological distribution of the genetic distances between trees. Moreover, *outbreaker2* assumes
55 mutation at transmission, thereby ignoring within-host evolution of the virus. A method that uses a phylogenetic
56 tree and within-host evolution is *Transphylo* [6], although transmission links are placed on a fixed phylogenetic tree.
57 Both *outbreaker2* and *Transphylo* can deal with unsampled cases within the population, which can be used to link
58 transmission clusters, although this is different than inferring introductions from an exogenous population. To model
59 multiple introductions from an exogenous population, Mollentze et al. [?] extended the transmission model of Morelli
60 et al. [20], which simultaneously infers a transmission and phylogenetic tree. Here, the within-host evolution was
61 modeled by the use of a binary tree, making the use of multiple samples per host problematic. Moreover and most
62 importantly, there is no publicly available software to use the method.

63 To make optimal use of genetic and epidemiological data while allowing for multiple introductions of a pathogen,
64 we propose a method to simultaneously infer introductions and transmissions consistent with an explicit phylogeny
65 describing the genetic history of all samples. This extended version of the method developed by Klinkenberg et al.
66 [18] aims to infer the transmission dynamics of an outbreak, i.e., who infected whom, from both genetic data of the
67 pathogen and epidemiological data, such as the time of sampling and culling. Inference of the transmission tree
68 and the phylogenetic tree is done simultaneously, concerning four processes: genetic diversity (within and between
69 transmission trees), within-host diversity, transmission, and case observation. Samples from posterior distributions
70 of the model parameters are taken, using a Markov-Chain Monte Carlo (MCMC) method. These samples provide
71 information on how likely certain infection times and infectors of hosts are.

72 To address the possibility of multiple introductions, we relax the assumption of a single index case. We add an
73 artificial host to the set of sampled hosts, which serves as an infector for all index cases (Figure 1). For this artificial
74 host, we introduce the term 'history host', referring to the representation of the history of the lineages within the index
75 cases. Using the history host, multiple outbreaks of a pathogen in the same population are merged into a single
76 phylogenetic tree.

77 After evaluation of the performance on simulated outbreaks with single and multiple introductions, we illustrate the
78 application of our method with an analysis of an outbreak of the SARS-CoV-2 virus in the Dutch mink farm industry.
79 From April to November 2020, 63 mink farms tested positive for SARS-CoV-2. To investigate whether the virus
80 was introduced several times into the mink population, we estimated the number of introductions and compared
81 the resulting transmission tree and phylogenetic tree to the phylogenetic tree obtained in [19, 21]. To describe
82 the generation time distribution of infected farms, we used a within-farm model of time since infection, that takes
83 measures to reduce the spread and culling of all animals into account. Furthermore, we implemented the possibility
84 to include multiple sequences per host.

85 Results

86 Modelling with the history host

87 To infer the transmission tree of an infectious disease outbreak, we developed a Bayesian method in which four
88 processes define the likelihood of a tree. Mutation events are modeled with a mutation rate μ . For the within-host
89 dynamics, we make a distinction between the history host and the sampled hosts. The history host represents
90 either a different population of the same host species, or a different host species (e.g., zoonotic infection), or an
91 environmental source. Therefore, it contains the evolution of the pathogen in the source population, with coalescence
92 happening on a different time scale than within the sampled hosts (see Figure 1). Coalescence, i.e. lineages
93 merging backward in time, is thus described by two rates: rate $1/r(\tau)$, with τ the time since infection, for the
94 coalescence events in the sampled hosts, and rate $1/r_{\text{history}}(\tau)$ for the coalescence events in the history host.
95 Timing of transmission is described by a generation time distribution, in the default model a gamma distribution
96 with mean m_G and shape a_G , and for the analysis of the mink farm data we used the generation time described in
97 the methods. Sampling time intervals, as a representation of case observations, are also described by a gamma
98 distribution with mean m_S and shape a_S .

99 Improving efficiency of the MCMC

100 The posterior is sampled by MCMC, with proposals that simultaneously change the phylogenetic and transmission
101 trees. In case there are many introductions, convergence of the MCMC chain to the optimal phylogenetic tree in
102 the history host is usually slow for a random initial configuration of the phylogenetic tree. We solved this issue
103 by (1) initializing the MCMC chain by making each host an introduction and using the neighbor-joining (NJ) tree
104 for the phylogenetic tree in the history host, and (2) implementing the parallelized Metropolis Coupled Monte Carlo
105 Markov Chain (p(MC³)) algorithm to give more freedom to the chain [1]. We tested for convergence by comparing
106 the likelihood reached by each algorithm, to the likelihood reached by an MCMC chain starting with the simulated
107 (true) phylogenetic and transmission trees. It turned out that the NJ initialization and the p(MC³) algorithm always
108 led to optimal convergence, whereas starting from a random tree and using MCMC sometimes ended up in a local
109 optimum, especially when the number of introductions is high (Table S1). As the tree estimated from the posterior
110 of an MCMC with random initialization did not converge optimally (Figure S1), we say that the configuration of the
111 history host is a bottleneck for performance. Trees may end up in a local optimum of the likelihood. To escape these
112 local optima all following analyses are done with NJ-tree initialization and p(MC³).

113 Varying number of introductions and coalescent rate

114 Before assessing in detail the method's performance to identify the correct introductions and infectors, we compared
115 its performance in relation to different priors. Outbreaks of with 20 hosts were simulated with 5 introductions and
116 a set of default parameters (see materials and methods). The outbreaks were analyzed with uninformative priors
117 on all parameters, informative priors on the mutation rate and mean generation and sampling intervals, and with all
118 parameters set to their true values. Results were compared with respect to identifying the correct infectors, infection
119 times, and parameter values. Only small differences were found between the results of each set of priors for the
120 outbreaks with 5 introductions (Table S2). For instance, the mean numbers of correctly identified infectors were 15,
121 15, and 15.7, with increasing prior information.

122 Next, we simulated outbreaks with varying numbers of introductions and varying coalescent rates of the history host.
123 While fixing the number of sampled hosts at 20, we simulated outbreaks with either 1, 2, 5, 10, 15, or 20 introductions.
124 For each number of introductions, we used coalescent rates of 0.004, 0.02, and 0.1 coalescence events per day in
125 the history host, against the background of a mean generation interval of 1 day for transmission events. Thereby
126 we changed the genetic variability of the index cases, by different coalescent rates in the history hosts, resulting in
127 different branch lengths in the phylogenetic tree in the history host. Each combination of a number of introductions
128 and coalescent rate was used for 25 simulated outbreaks, resulting in 450 outbreaks. We analyzed the simulated
129 data with informative priors (Table S2), as in outbreak research most of the time there is some prior information about
130 the generation time and mutation rate.

131 Analyzing simulated outbreaks with 1 introduction resulted in a mean number (of 25 posterior medians) of 1
132 introduction, see Figure 2A. This result did not change with the coalescent rate, because there is no coalescence in
133 the history host. With 2 or 5 introductions, the estimated medians were still close to the simulated number. However,
134 with 10 or more introductions the estimated medians were lower than the simulated number of introductions, and a
135 high coalescent rate increased this gap. When all hosts are simulated as an introduction, no more than 40% of all
136 introductions were truly identified by the inference method. This indicates that simulated clusters were merged due
137 to the low genetic variability.

138 Approximately 70% of all hosts have correctly identified infectors when there was 1 introduction, and more than 95%
139 of the hosts had their true infectors present in the 95% support set (Figure 2B). This is the set of infectors for a host
140 with cumulative support of at least 95%, with infectors added by decreasing support. For more introductions and
141 low coalescent rates, more infectors were correctly identified, whereas for higher coalescent rates the number of
142 correctly identified infectors decreased.

143 Several types of incorrectly identified infectors can be distinguished. We define a transmission cluster as the set of
144 hosts derived from one index case. We separate the errors into two classes: involving a single transmission cluster
145 in both the simulated and estimated tree (single, S), or involving multiple transmission clusters in the simulated
146 and/or estimated tree (multiple, M). The simulated or identified infector is then in a different transmission cluster than
147 the case in the simulated or estimated tree. Both classes of error can be subdivided into three subclasses: both
148 simulated and identified infectors are other cases in the data set (case to case, C->C), the simulated infector is the
149 history host and the identified infector is a case (history to case, H->C), and the simulated infector is a case and the
150 identified infector is the history host (case to history, C->H) (see Figure S1). In our analysis, we find that for small
151 numbers of introductions, i.e. 1, 2, and 5, almost all errors are within a single transmission cluster and do not involve
152 an index case (single none). For 10 introductions, this is around half of the errors, while the other half are merges of
153 transmission clusters (multiple simulated). Larger numbers of introductions, i.e. 15 and 20, mostly lead to merged
154 transmission clusters. With the number of introductions approaching the number of sampled hosts, there are only
155 very few transmission events, such that it is hard to estimate the mutation rate or the coalescent rate in the history
156 host correctly. An overestimation of the mutation rate, or an underestimation of the coalescent rate, makes it more
157 likely that index cases are placed in the same cluster, causing merges. Fewer index cases imply more transmission
158 events to estimate the correct parameter values. However, even if all parameters were fixed at their true value, an
159 incorrect infector sometimes has the highest posterior probability (Figure S2).

160 So, for low numbers of introductions, in these simulations up to 5, the model can reliably infer the number of
161 introductions when informative priors are given for the model parameters. The number of introductions tends to
162 be underestimated if there are many, due to the merging of clusters.

163 SARS-CoV-2 in mink farms: analysis of simulated data

164 In 2020, an outbreak of SARS-CoV-2 occurred among mink farms in the Netherlands. Symptomatic infections in
165 minks first occurred two months after the virus was introduced into the Dutch human population, which suggests that
166 the outbreak was a spillover from humans to mink. To investigate whether there were multiple introductions of the
167 virus into the mink farm population, we applied our extended method to sequence data collected from minks together
168 with their time of sampling. Culling times of the farms were also known. To assess the accuracy of our method on
169 outbreaks with sizes similar to the SARS-CoV-2 outbreak, we simulated and analyzed outbreaks with comparable
170 settings (see material and methods). Again, we tested different numbers of introductions, for which 10 outbreaks
171 each were simulated and analyzed. The results are shown in Table 1. Compared to the percentages of correctly
172 identified infectors for outbreaks with 20 hosts, the model performs equally well for the larger outbreak size of 63
173 hosts. Around 70-75% of all infectors are correctly identified with the highest support, and the true infector of a host
174 is present in the 95% CI set for at least 95% of all hosts. Only for a high number of introductions (e.g., 20, or 30
175 introductions), the performance decreases, due to merged clusters, with 5-10% (Figure S3).

176 SARS-CoV-2 in mink farms: analysis of the Dutch outbreak

177 During the first and second wave of SARS-CoV-2 infections in the Netherlands (starting in March 2020 and
178 September 2020 respectively), 63 out of a total of 126 mink farms in the Netherlands were sampled positive for
179 the virus. From the end of April 2020 till November 2020, genetic and epidemiological data were collected on these
180 farms, including viral sequences, sampling times, and culling times. A phylogenetic analysis of the viral sequences
181 showed 5 distinct genetic clusters of farms, based on their separation by sequences from human samples [19].
182 Classification by PANGO lineages [24] showed that each cluster contained one PANGO lineage, with 2 clusters
183 containing the same lineage (Table S?). One farm, NB-EMC-8, contained samples from 2 different clusters and is
184 therefore split into NB-EMC-8a and NB-EMC-8b in our analysis. Whereas the phylogenetic analysis could distinguish
185 five clusters based on human intermediate samples, suggesting five introductions, it could not rule out multiple
186 introductions within each cluster. For an estimate of the number of introductions without the need for intermediate
187 samples from the source population, we analyzed this outbreak with our extended version of phylbreak. We set the
188 following priors on the model parameters: $\mu_\mu = 3 \cdot 10^{-6}$ substitutions per nucleotide per day, $\sigma_\mu = 1 \cdot 10^{-6}$ [2] and
189 the mean $r_{\text{history}} = 20$ coalescent events per day with shape equal to 3 (see materials and methods). The mean of
190 the prior introduction rate distribution is 5/180, as five genetic clusters were reported within 180 days, with shape
191 equal to 3. Finally, we set the prior mean sampling time μ_S at 10 days, with standard deviation $\sigma_S = 2$, as infection
192 is expected to happen 1-2 weeks before sampling [11].

193 The method estimated the time of the first coalescent event in the history host on March 4th, 2020 (Table 2). The
194 reduction factor of infectiousness after sampling L was estimated at 1, meaning that the method did not find an
195 influence of sampling on infectiousness. We find 13 introductions in the maximum parent credibility tree (see Figure
196 3), of which 11 have minimal support above 0.5. The median number of introductions in all cycles was 13, with
197 the first and third quartile being 11 and 14 introductions respectively (Figure S7). Six introductions initiated a
198 transmission chain, whereas the other 7 were single cases. By coloring the host labels, we see that the method
199 divided the hosts into subtrees similar to the phylogenetic clusters found by Lu et al. [19]. Two genetic clusters,
200 i.e. cluster B and cluster D, were merged into a single transmission cluster, and with a genetic distance of only 4
201 nucleotides they belong to the same PANGO lineage. Genetic cluster C is split into two transmission clusters, with
202 NB-EMC-46 as the index case of one of them. NB-EMC-46 was placed in genetic cluster A, but its samples were
203 found to belong to multiple PANGO lineages, including the lineage of genetic cluster C. This indicates that farm
204 NB-EMC-46 is infected multiple times. The large genetic cluster A is separated into multiple transmission clusters,
205 meaning that not all genetically clustered farms are linked by one transmission chain. We find that the single cases
206 which are part of this phylogenetic cluster have common ancestors with cases in the human population (Figure S5).
207 Time of infection and genetic distance made it less likely that the single farms were part of the transmission cluster
208 of farms. In the later stage of the outbreak, there are two larger transmission chains, for which the exact index case
209 is less certain (Figure S8). There is support for the scenario that these transmission clusters are merged into one. In
210 conclusion, by using a phylodynamic model combining the phylogenetic history of the samples with the transmission
211 history between the farms, we were able to distinguish farm-to-farm transmission routes within a group of farms with
212 a common introduction from the human population.

213 Our extensions are implemented in the package *phybreak* [18] for the R software [26] and can be found at
214 <https://github.com/bastiaanvdroest/phybreak>. The package version used, together with the code for the analyses,
215 is found at https://github.com/bastiaanvdroest/phybreak_multiple_introductions.

216 Discussion

217 The method presented enables for the first time to simultaneously estimate the phylogenetic tree and the
218 transmission tree of an outbreak in the case where there may have been multiple introductions. The inference is
219 done without breaking the dependencies between mutations, within-host dynamics, transmission, and observation.
220 By modeling the history of lineages infecting index cases through a phylogenetic tree in a history host, we can
221 distinguish between single and multiple introductions. As an extension to the model of Klinkenberg et al. [18],
222 we now have an easily accessible method for transmission tree inference, with the possibility to assess multiple
223 introductions.

224 From analyses of simulated outbreaks, we conclude that the model can infer the true number of introductions if there
225 are few introductions compared to the total outbreak size. For an increasing number of introductions, the model
226 increasingly underestimated the number of introductions, but the posterior distribution did include the actual number
227 of introductions. The simulated index cases which were incorrectly identified as non-index cases did have support
228 as an index in the posterior trees. This means that interpretation of the transmission trees should take into account
229 the support as index for cases.

230 The ability to infer multiple introductions in the analysis of an outbreak is not only useful for finding transmission
231 clusters but also gives valuable information on how to respond to an outbreak. In the case of multiple introductions,
232 measures aimed at reducing transmission events need to be complemented by preventing introduction from outside
233 the target population. Therefore it is of great importance to distinguish between single and multiple introductions
234 of a pathogen in a population. With simulated data sets, we showed that our method is a useful tool to make this
235 distinction: outbreaks with a single introduction are almost always inferred to have a single index case, and outbreaks
236 with multiple introductions are almost never inferred to have a single introduction.

237 Although the model can distinguish between single or multiple introductions, the accuracy strongly depends on
238 genetic variability. High genetic variability makes it easier to distinguish clusters of hosts, and thus gives more
239 weight to the true number of introductions in the posterior. Low genetic variability, however, will cause sub-trees to
240 be merged and therefore will lead to an underestimation of the number of introductions. As this variability depends
241 on the variation in the external source population, which depends on the mutation rate and effective population size
242 in the history host, it is not possible to state in beforehand how accurate the results will be. When available, strong
243 priors on the mutation rate and coalescent rate in the history host will increase the accuracy, although even with the
244 true values of the model parameters sub-trees will not always be separated. In that case, there is too little information
245 in the genetic and epidemiological data to find all introductions.

246 Transmission clusters of an infectious disease outbreak in a population are often derived with phylogenetic analyses.
247 However, with closely related index cases, defining clusters may become arbitrary. If obtainable sequences sampled
248 outside of the study population may help to discriminate the clusters by acting as 'missing links' between clusters,
249 but discrimination is not so likely if clusters are closely connected. As with the SARS-CoV-2 outbreak in minks, low
250 genetic variability may cause transmission clusters to be merged in the phylogenetic tree, thereby underestimating
251 the number of introductions. We have shown that our method can be used as an alternative approach, which only
252 depends on the genetic data from the study population. Moreover, with the addition of epidemiological data, e.g.
253 sampling times and culling times, it can differentiate genetically similar transmission clusters.

254 Application of the model to a SARS-CoV-2 outbreak in the Dutch mink farms led to confirmation of previously found
255 phylogenetic clusters, although the phylogenetic clusters are broken down into multiple transmission clusters. These
256 transmission clusters are composed of individual infections along with a larger transmission tree. We split farm
257 NB-EMC-8 based on the genetic clustering of the samples taken on this farm. Without this split, a transmission
258 cluster would have been formed containing multiple PANGO lineages and always having NB-EMC-8 separating the
259 two genetic clusters within that transmission cluster. Farm NB-EMC-46 is also likely to be infected multiple times,
260 as in our results it is the index case of a transmission cluster containing samples from a different genetic cluster
261 than NB-EMC-46. Currently, our method does not allow for multiple infections of a host with different strains, and
262 therefore these clusters could not be separated by the estimation procedure. Extending the method to allow multiple
263 infections of the same host is a challenge for future development. The SARS-CoV-2 outbreak on the mink farms has
264 been studied previously in which samples of humans around and on the farms were used. Here we show that we
265 come to similar conclusions, but do not need samples of the source population to distinguish transmission clusters.
266 Often such data is not available, for example with introductions from other countries, the general population is case
267 of non-notifiable diseases or from wildlife.

268 The possibility to distinguish multiple introductions of a pathogen into a host population opens up a new avenue for
269 the analysis of outbreaks. However, the method assumes a large population of which a small part gets infected and
270 where contact is equally likely for all pairs of hosts. An outbreak on, for instance, a hospital ward does not meet
271 this assumption with its small population size, in and outflow of patients, and spatial distance between patients. To
272 address these assumptions, the population size has to be accounted for, and contact data, i.e., possible (in)direct

273 contacts between hosts, as well as the geographical location of hosts give a probability of the contact between hosts.
274 Transmission routes can be excluded based on these data sources, such that the certainty of the results increases.
275 In conclusion, we developed a new method for transmission tree inference which makes it possible to estimate the
276 number of introductions of a pathogen during an outbreak. the analysis of the SARS-Cov-2 outbreak in Dutch mink
277 farms shows multiple introductions of the virus, indicating that even with fully controlling farm-to-farm transmission,
278 newly infected farms would arise by new introductions from the human population. Our method opens the way to
279 evaluate outbreaks in such a way that information about new introductions can be derived; knowledge that is useful
280 for policy-making.

281 Methods

282 Tree inference model

283 The transmission and phylogenetic tree inference model describes the likelihood of observing an infectious disease
 284 outbreak based on the epidemiological and genetic links between hosts and samples. The outbreak dynamics are
 285 described by four processes: incidence of new cases by introduction from outside or transmission by existing cases,
 286 the observation of the pathogen through sampling, the dynamics of the pathogen within infected hosts and the
 287 history host, and genetic mutations in the pathogen. By means of MCMC, we sample from the posterior distribution
 288 of parameters and phylogenetic and transmission trees, formed by prior distributions and four likelihood functions
 289 for the four processes. The inference is done by a Bayesian analysis, using Markov-Chain Monte Carlo (MCMC) to
 290 obtain samples from the posterior distributions of all outbreak parameters and transmission events. We will briefly
 291 summarize the likelihood functions, the posterior distributions, and the update steps in the MCMC chain.

292 Incidence of cases after the first introduction is modeled by two independent processes: additional introduction from
 293 outside the study population and transmission between hosts. Additional introductions occur with a rate λ_{intro} , after
 294 the first introduction until the last sample time. We denote by T the time between the first introduction and the last
 295 sample time, and k the number of introductions. Transmission occurs with a dynamic rate, depending on the times
 296 since infection of infected hosts, described by the generation time distribution. This is a Gamma distribution with
 297 shape a_G and mean m_G . By the use of vector \mathbf{I} of all infection times, including introductions, and the numeric vector
 298 \mathbf{M} indicating the infectors of all hosts and 0 for introductions, the probability density function of the generation time
 299 of a host i , with $M_i \neq 0$, is $d_{\Gamma(a_G, m_G)}(I_i - I_{M_i})$. The likelihood for the transmission tree is therefore:

$$\Pr(\mathbf{I}, \mathbf{M} | a_G, m_G) = \lambda_{\text{intro}}^{k-1} \cdot e^{(-\lambda_{\text{intro}} * T)} \cdot \prod_{i | M_i > 0} d_{\Gamma(a_G, m_G)}(I_i - I_{M_i})$$

303 For sampling, we assume that all hosts are detected and sampled at random times after they were infected, according
 304 to a Gamma distribution with shape a_S and mean m_S . The likelihood uses the vector S of sampling times of all hosts
 305 and is therefore:

$$\Pr(\mathbf{S} | \mathbf{I}, a_S, m_S) = \prod_i d_{\Gamma(a_S, m_S)}(S_i - I_i)$$

307 The phylogenetic tree P describes the evolutionary history of all sampled sequences and is built from the
 308 phylogenetic mini-trees for each host, connected through the transmission links. The introductions are connected
 309 by a phylogenetic tree in a separate 'history host'. Each mini-tree has tips formed by samples and lineages from
 310 secondary cases, and a single root which is a tip in the mini-tree of the infector. Mini-trees are formed by coalescent
 311 processes. In (normal) hosts, a rate $1/w(\tau, r)$ describes coalescence between any pair of lineages within the host
 312 going backward in time; in the history host, the rate is constant over time: r_{history} . In our analysis, we use $w(\tau, r) = r\tau$,
 313 the linearly increasing within-host pathogen population size at forward time τ since infection of the host. In the
 314 phylogenetic tree P of the outbreak with the set of nodes V , there are three sets of nodes: sampling nodes V_S , i.e.
 315 the tips of the tree where sampling took place, coalescent nodes V_C and transmission nodes V_T , where a lineage
 316 goes from the infector to its infectee. For node x , τ_x gives the time of the node since infection of the host. The
 317 number of lineages in host i at time τ is then denoted by $L_i(\tau)$:

$$L_i(\tau) = 1 + \sum_{\substack{x \in P_i \\ x \in V_C}} (u(\tau - \tau_x)) - \sum_{\substack{x \in P_i \\ x \in (V_T \cup V_S)}} (u(\tau - \tau_x))$$

319 where $u(\tau)$ is the heaviside step function, i.e. $u(\tau) = 0$ if $\tau < 0$, and $u(\tau) = 1$ if $\tau \geq 0$. The likelihood of each host's
 320 tree is then

$$\Pr(P_i | S_i, \mathbf{I}, \mathbf{M}, r) = \exp\left(-\int_0^\infty \binom{L_i(\tau)}{2} \frac{1}{w(\tau, r)} d\tau\right) \cdot \prod_{\substack{x \in P_i \\ x \in V_C}} \frac{1}{w(\tau_x, r)}$$

322 with $\binom{0}{2} \equiv \binom{1}{2} \equiv 0$. Here, the first term is the probability to have no coalescent event during the intervals in which
 323 there are two or more lineages, and the second term is the product of coalescent rates at the coalescent nodes.
 324 The prior distribution of the slope r is Gamma distributed with shape a_r and rate b_r . Those were set to $a_r = b_r = 3$

325 in an uninformative analysis. For the history host, we assume that the coalescent rate is constant over time, so
 326 $w(\tau, r_{hist}) = r_{hist}$. The total likelihood of the within-host dynamics is the product of all hosts' likelihoods:

$$\Pr(P|\mathbf{S}, \mathbf{I}, \mathbf{M}, r) = \Pr(P_0|\mathbf{I}, \mathbf{M}, r_{history}) \cdot \prod_{i|i>0} \Pr(P_i|S_i, \mathbf{I}, \mathbf{M}, r)$$

328 Mutations are described by a Jukes-Cantor model, stating that any of the four nucleotides have equal probability to
 329 mutate to, with a fixed mutation rate μ for all sites in the set of sequences \mathbf{G} . For all coalescent and transmission
 330 nodes x , which occur at time t_x with parent node v_x , the mutation likelihood is:

$$\Pr(\mathbf{G}|P, \mu) = \prod_{loci \{A, C, G, T\}^{3n-1}} \prod_x \left(\frac{1}{4} - \frac{1}{4} \exp(-\mu(t_x - t_{v_x})) \right)^{\mathcal{I}_{mut}(1-N)} \cdot \left(\frac{1}{4} + \frac{3}{4} \exp(-\mu(t_x - t_{v_x})) \right)^{(1-\mathcal{I}_{mut})(1-N)}$$

332 Here, \mathcal{I}_{mut} indicates if a mutation occurred on the branch between x and v_x , and N indicates if a branch ends with a
 333 tip with an unknown nucleotide ('n' in the sequence). We use here a strict molecular clock model, i.e. one mutation
 334 rate for all branches of the phylogenetic tree, because on this time scale there won't any effect of different mutation
 335 rates. In the history, changes of mutation rates are met by the coalescent rate of the history host. The likelihood is
 336 calculated using Felsenstein's pruning algorithm [8].

337 The transmission tree and its parameters are inferred by a Bayesian analysis, using Markov-Chain Monte Carlo
 338 (MCMC). From the MCMC we obtain samples from the posterior distributions of the model parameters, the infectors,
 339 and the infection times of all hosts. The posterior distribution, with θ the set of model parameters, is given by

$$\Pr(\mathbf{I}, \mathbf{M}, P, \theta | \mathbf{S}, \mathbf{G}) \propto \Pr(\mathbf{G}|P, \theta) \cdot \Pr(P|\mathbf{S}, \mathbf{I}, \mathbf{M}, \theta) \cdot \Pr(\mathbf{S}|\mathbf{I}, \theta) \cdot \Pr(\mathbf{I}, \mathbf{M}|\theta) \cdot \Pr(\theta)$$

341 MCMC sampling

342 An MCMC chain is run to get the posterior distribution of the model parameters, together with the transmission and
 343 phylogenetic tree of the outbreak. The MCMC chains were initialized by first choosing the means of priors for the
 344 parameters (except for μ), then constructing the transmission and phylogenetic trees, and finally computing a value
 345 for μ . The trees were constructed by first sampling infection times from the observed sampling times and sample
 346 time distribution. All cases were assumed to be index cases (other options are possible within the package), and
 347 the topology of the phylogenetic tree was made with the neighbor-joining algorithm using the first sequence of each
 348 host. The times of the coalescent nodes were simulated with the coalescent model. This guaranteed an optimized
 349 tree topology in the history host, not needing to be reached by sampling in the MCMC chain. The parameter μ was
 350 for the initial state set to be the tree parsimony (the number of mutations on the tree) divided by the sum of all branch
 351 lengths and the genome size. The default prior distributions for the model parameters are found in Table 3. The
 352 priors for m_G and m_S are translated into a prior for the rate parameter in the Gamma distribution. More detail about
 353 the prior and posterior distributions is included in the supplementary material. Per iteration cycle, each host is picked
 354 once in random order as the focal host. A new infection time I'_i is proposed for focal host i and consecutive steps
 355 are made according to this new infection time. At the start of a proposal, there are two main ways of updating: within
 356 a sub-tree, by following all hosts with a common index case along their transmission links, or between sub-trees.
 357 Here we will describe the proposal step for updating between sub-trees, as this is the step where the number of
 358 introductions can be altered. The update steps within a sub-tree are as in the original *phybreak* package and can be
 359 found in the supplementary information.

360 Three situations describe the possibility to update the transmission tree between sub-trees (see figure 4):

- 361 1. The focal host i is the history host. In this case, new coalescent times are proposed. Optionally, a new
 362 phylogenetic mini-tree can be proposed.
- 363 2. The focal host i is an index case. An infection time I'_i is proposed. If this I'_i is before the first transmission from
 364 host i , a new infector M'_i is proposed out of the hosts which are infectious at time I'_i . Two situations are now
 365 possible:

- 366 a If $M_i^I = 0$, then host i remains an index case, with infection time I_i^I .
- 367 b If $M_i^I \neq 0$, then host i is no longer an index case, and there is one introduction less. Host i and its
- 368 descendants will be merged as a branch to another sub-tree.
- 369 3. The focal host i is not an index case. An infection time I_i^I is proposed. If this I_i^I is before the first transmission
- 370 from host i , a new infector M_i^I is proposed out of the hosts which are infectious at time I_i^I . Two situations are
- 371 now possible:
- 372 a If $M_i^I = 0$, then host i will become an index case, and there is one extra introduction. The new sub-tree
- 373 consists of host i and all of its descendants.
- 374 b If $M_i^I \neq 0$, then host i either switch to another branch in its sub-tree or switch to another sub-tree. There
- 375 is no change in the number of introductions.

376 Each proposal step is followed by proposing new phylogenetic mini-trees for all hosts involved. The proposal

377 distributions and acceptance probabilities of all steps are described in the supplemental materials. The MCMC

378 chain is run according to the $(MC)^3$ algorithm described by Altekar et al.[1] to improve convergence to the global

379 likelihood optimum. The chains consisted of 35,000 cycles of which the first 10,000 were used as burn-in.

380 Construction and analysis of simulated outbreaks

381 To verify the implementation of multiple introductions in the model, we simulated outbreaks including one or more

382 index cases, and analyzed them by running MCMC chains. The simulation of an outbreak starts with the simulation

383 of a transmission tree:

- 384 1. Set an observation size, i.e. the number of hosts, the number of introductions k , and the duration of the
- 385 outbreak T .
- 386 2. Calculate the optimal population size in which to simulate the outbreak from parameter R_0 and the observation
- 387 size.
- 388 3. Sample $k - 1$ introduction times from the exponential waiting time distribution with rate λ_{intro} . The introduction
- 389 time of the first index case will be 0, and other introductions are at cumulative waiting times from the first index.
- 390 4. For the index cases, sample the number of secondary cases from a Poisson distribution with parameter R_0 .
- 391 5. The generation time between two hosts is Gamma distributed with shape a_G and mean m_G . After infection,
- 392 the sampling of a host takes place after a Gamma distributed time with shape a_S and mean m_S .
- 393 6. Repeat steps 3 and 4 for the complete population size, where the infection time for a host is not after T .
- 394 Remove non-index cases without any links.
- 395 7. Repeat 3-6 till the desired observation size was given.
- 396 8. Add the history host and connect the index cases to this host.

397 After the simulation of the transmission tree, the phylogenetic tree is constructed by simulating phylogenetic

398 mini-trees for each host. Coalescent times are sampled according to the given coalescent rate $1/w(\tau, r)$. Edges

399 between sample, coalescent, and transmission nodes are made backward in time. In the history host, coalescence

400 events occur with a constant rate $1/r_{\text{history}}$.

401 For the sequences, we sample the number of mutations from a Poisson distribution with parameter equal to $\lambda =$

402 $\mu \cdot \text{sequence length} \cdot \text{total length of all edges}$, where μ is the mutation rate. The mutations are distributed over the

403 edges, with weights the lengths of the edges. For each mutation, a uniform random locus is changed to a uniform

404 random nucleotide.

405 We simulated outbreaks with a basic set of parameter values, the same as in Klinkenberg et al. [18], ($m_G = 1$, $a_G =$

406 10 , $m_S = 1$, $a_S = 10$, $R_0 = 1.5$, $r = 1$, a sequence length of 10^4 nucleotides and a mutation rate of $\mu = 10^{-4}$), with

407 new parameters at $\lambda_{\text{intro}} = 1$. The number of introductions varied between the simulations to assess the performance

408 of the model. MCMC chains were run following the $(MC)^3$ algorithm, with 3 parallel chains with heats 1, 0.5, and

409 0.333. The chains are 35,000 cycles long, of which the first 10,000 cycles are used as burn-in. Posterior distributions

410 for infectors, infection times, and model parameters are collected from the remaining 25,000 cycles.

411 Analysis of SARS-CoV-2 outbreak in Dutch mink farms

412 As an application of the method, we analyzed the SARS-CoV-2 outbreak in the Dutch mink industry in 2020 [19].
413 We collected the full viral genomes in minks at 63 farms from GISAID (gisaid.org) and aligned them with MUSCLE
414 [7]. The alignment contains 326 sequences of 29,775 nucleotides long. All positions with N in all 326 sequences are
415 removed because we do not know if there is a mutation at such a position. This left us with 326 sequences of 16,289
416 nucleotides long. Each farm is sampled at least once, and we have an average number of 5 samples per farm, each
417 farm sampled on a single day. Besides the date of sampling, we also have the date of culling, which is between 1
418 day and 45 days after sampling, with an average of 4 days. The first 5 farms found to be infected had more than 30
419 days between sampling and culling, but for the rest of the farms, this was no more than 10 days.

420 We described the outbreak among mink farms by taking the farms as hosts. The prior distributions of the model
421 parameters are set as follows: we set the mean sampling time interval $m_S = 10$ days (with a shape $a_S = 3$), as
422 the time between infection and detection was estimated to be 1-2 weeks [11]. We set the mean introduction rate to
423 $5/180$ (with a shape of 3), as five different clusters were found during the outbreak, which lasted for approximately
424 180 days, by Lu et al. [19]. The coalescent rate parameter r_{history} was set to 20. With an expected number of 5
425 introductions, this rate represented the introduction of the virus in the Netherlands two months before the first positive
426 mink sample. The other prior distributions were set to default.

427 As the hosts are farms here, we introduced an infectiousness function describing the growth and circulation of the
428 virus within the mink population of a farm. This function replaced the gamma distribution for the likelihood that one
429 farm infected another. We assumed that infectiousness follows a logistic curve, with a reduced level after detection
430 at time T_s , and exponential decline after culling at time T_c :

$$431 \quad I = \begin{cases} \frac{1}{1 + ae^{-gt}} & t < T_s \\ \frac{L}{1 + ae^{-gt}} & T_s < t < T_c \\ \frac{L}{1 + a \cdot e^{-gT_c}} \cdot e^{-C(t-T_c)} & t > T_c \end{cases}$$

432 Here, $a = 1 \cdot 10^{-4}$ is the initial part of the mink population at a farm being infected, g is the growth rate, and t is the
433 time after infection of the farm. Parameter L is estimated to see if there was some reduction of infectiousness after
434 detection, and C is a fixed value. Because the values for T_s and T_c differ per farm, the infectiousness curves differ
435 between the farms. Therefore we normalize the curves, such that the mean AUC of all curves is 1. Then, on average
436 a farm has a distribution of infectiousness that adds up to 1, just as in the default *phybreak* model, while accounting
437 for higher total infectivity of longer infected farms. Another addition used for the mink farms was to include multiple
438 samples per farm. Phylogenetic mini-trees are then built with multiple lineages within a farm, increasing the amount
439 of genetic data. For the sampling time distribution, only the first sample of each host is used.

440 To test the new model, with a similar history host, and sampling time distribution, we simulated outbreaks with the
441 same parameters as before but with the new infectiousness curve. Culling times were set 15 days after infection,
442 such that the hosts have a fixed infectiousness curve. As for the outbreak size, we used 63 hosts with 1 sample per
443 host. Prior distributions were set with the same parameter values as the analysis of the real data. We set C to 5,
444 such that in 5 days after culling the infectiousness of a farm was 0. We varied the number of introductions, from 1,
445 2, 5, 10, 20, up to 30 introductions. Results of the SARS-CoV-2 outbreak were obtained by running three parallel
446 chains, with 25,000 cycles each, according to the $(MC)^3$ algorithm. The maximum parent credibility tree is used for
447 visualization, computation of the number of introductions, and comparison to the phylogenetics [19].

448 **Acknowledgments**

449 This work was performed as part of the research program of the Netherlands Centre for One Health (www.ncoh.nl).
450 We thank Bas Oude Munnik, Francisca Velkers and the 'One Health mink outbreak investigation consortium' for
451 providing a prepublication of the mink data.

References

- 453 1. Altekar, G., Dwarkadas, S., Huelsenbeck, J. P., and Ronquist, F. Parallel Metropolis coupled Markov chain Monte Carlo for
454 Bayesian phylogenetic inference. *Bioinformatics*, 20(3):407–415, 2004. doi: 10.1093/bioinformatics/btg427.
- 455 2. Amicone, M., Borges, V., Alves, M. J., Isidro, J., Zé-Zé, L., Duarte, S., Vieira, L., Guiomar, R., Gomes, J. P., and Gordo, I.
456 Mutation rate of SARS-CoV-2 and emergence of mutators during experimental evolution. *Evolution, Medicine, and Public
457 Health*, 10(1):142–155, 1 2022. doi: 10.1093/emph/eoac010.
- 458 3. Cauchemez, S. and Ferguson, N. M. Methods to infer transmission risk factors in complex outbreak data. *Journal of the
459 Royal Society, Interface*, 9(68):456–69, 3 2012. doi: 10.1098/rsif.2011.0379.
- 460 4. Cauchemez, S., Boelle, P.-Y., Donnelly, C. A., Ferguson, N. M., Thomas, G., Leung, G. M., Hedley, A. J., Anderson, R. M.,
461 and Valleron, A.-J. Real-time estimates in early detection of SARS. *Emerging infectious diseases*, 12(1):110–3, 1 2006. doi:
462 10.3201/eid1201.050593.
- 463 5. Didelot, X., Gardy, J., and Colijn, C. Bayesian inference of infectious disease transmission from whole-genome sequence
464 data. *Molecular Biology and Evolution*, 2014. doi: 10.1093/molbev/msu121.
- 465 6. Didelot, X., Fraser, C., Gardy, J., Colijn, C., and Malik, H. Genomic infectious disease epidemiology in partially sampled and
466 ongoing outbreaks. *Molecular Biology and Evolution*, 34(4):997–1007, 4 2017. doi: 10.1093/molbev/msw275.
- 467 7. Edgar, R. C. MUSCLE: multiple sequence alignment with high accuracy and high throughput. *Nucleic Acids Research*, 32
468 (5):1792–1797, 3 2004. doi: 10.1093/nar/gkh340.
- 469 8. Felsenstein, J. Evolutionary trees from DNA sequences: A maximum likelihood approach. *Journal of Molecular Evolution*,
470 17(6):368–376, 11 1981. doi: 10.1007/BF01734359.
- 471 9. Fraser, C., Donnelly, C. A., Cauchemez, S., Hanage, W. P., Van Kerkhove, M. D., Hollingsworth, T. D., Griffin, J., Baggaley,
472 R. F., Jenkins, H. E., Lyons, E. J., Jombart, T., Hinsley, W. R., Grassly, N. C., Balloux, F., Ghani, A. C., Ferguson, N. M.,
473 Rambaut, A., Pybus, O. G., Lopez-Gatell, H., Alpuche-Aranda, C. M., Chapela, I. B., Zavala, E. P., Guevara, D. M. E.,
474 Checchi, F., Garcia, E., Hugonnet, S., and Roth, C. Pandemic Potential of a Strain of Influenza A (H1N1): Early Findings.
475 *Science*, 324(5934):1557–1561, 6 2009. doi: 10.1126/science.1176062.
- 476 10. Hall, M., Woolhouse, M., and Rambaut, A. Epidemic Reconstruction in a Phylogenetics Framework: Transmission Trees as
477 Partitions of the Node Set. *PLoS Computational Biology*, 11(12):1–36, 2015. doi: 10.1371/journal.pcbi.1004613.
- 478 11. Hammer, A. S., Quaade, M. L., Rasmussen, T. B., Fonager, J., Rasmussen, M., Mundbjerg, K., Lohse, L., Strandbygaard,
479 B., Jørgensen, C. S., Alfaro-Núñez, A., Rosenstjerne, M. W., Boklund, A., Halasa, T., Fomsgaard, A., Belsham, G. J.,
480 and Bøtner, A. SARS-CoV-2 Transmission between Mink (*Neovison vison*) and Humans, Denmark. *Emerging Infectious
481 Diseases*, 27(2):547–551, 2 2021. doi: 10.3201/eid2702.203794.
- 482 12. Harris, S. R., Feil, E. J., Holden, M. T. G., Quail, M. A., Nickerson, E. K., Chantratita, N., Gardete, S., Tavares, A., Day, N.,
483 Lindsay, J. A., Edgeworth, J. D., de Lencastre, H., Parkhill, J., Peacock, S. J., and Bentley, S. D. Evolution of MRSA During
484 Hospital Transmission and Intercontinental Spread. *Science*, 327(5964):469–474, 1 2010. doi: 10.1126/science.1182395.
- 485 13. Haydon, D. T., Chase-Topping, M., Shaw, D. J., Matthews, L., Friar, J. K., Wilesmith, J., and Woolhouse, M. E. J. The
486 construction and analysis of epidemic trees with reference to the 2001 UK foot-and-mouth outbreak. *Proceedings. Biological
487 sciences*, 270(1511):121–7, 1 2003. doi: 10.1098/rspb.2002.2191.
- 488 14. Jombart, T., Cori, A., Didelot, X., Cauchemez, S., Fraser, C., and Ferguson, N. Bayesian Reconstruction of Disease
489 Outbreaks by Combining Epidemiologic and Genomic Data. *PLoS Computational Biology*, 10(1), 2014. doi: 10.1371/
490 journal.pcbi.1003457.
- 491 15. Kenah, E., Britton, T., Halloran, M. E., and Longini, I. M. Molecular Infectious Disease Epidemiology: Survival Analysis
492 and Algorithms Linking Phylogenies to Transmission Trees. *PLoS computational biology*, 12(4):e1004869, 4 2016. doi:
493 10.1371/journal.pcbi.1004869.
- 494 16. Kenah, E. Semiparametric Relative-risk Regression for Infectious Disease Transmission Data. *Journal of the American
495 Statistical Association*, 110(509):313–325, 3 2015. doi: 10.1080/01621459.2014.896807.
- 496 17. Kerfua, S. D., Shirima, G., Kusiluka, L., Ayebazibwe, C., Mwebe, R., Cleaveland, S., and Haydon, D. Spatial and
497 temporal distribution of foot-and-mouth disease in four districts situated along the Uganda-Tanzania border: Implications
498 for cross-border efforts in disease control. *The Onderstepoort journal of veterinary research*, 85(1):e1–e8, 8 2018. doi:
499 10.4102/ojvr.v85i1.1528.
- 500 18. Klinkenberg, D., Backer, J. A., Didelot, X., Colijn, C., and Wallinga, J. Simultaneous inference of phylogenetic and
501 transmission trees in infectious disease outbreaks. *PLoS Computational Biology*, 13(5), 5 2017. doi: 10.1371/journal.
502 pcbi.1005495.
- 503 19. Lu, L., Sikkema, R. S., Velkers, F. C., Nieuwenhuijse, D. F., Fischer, E. A., Meijer, P. A., Bouwmeester-Vincken, N., Rietveld,
504 A., Wegdam-Blans, M. C., Tolsma, P., Koppelman, M., Smit, L. A., Hakze-van der Honing, R. W., van der Poel, W. H., van der
505 Spek, A. N., Spierenburg, M. A., Molenaar, R. J., Rond, J. d., Augustijn, M., Woolhouse, M., Stegeman, J. A., Lycett, S.,
506 Oude Munnink, B. B., and Koopmans, M. P. Adaptation, spread and transmission of SARS-CoV-2 in farmed minks and
507 associated humans in the Netherlands. *Nature Communications*, 12(1), 12 2021. doi: 10.1038/s41467-021-27096-9.
- 508 20. Morelli, M. J., Thébaud, G., Chadœuf, J., King, D. P., Haydon, D. T., and Soubeyrand, S. A Bayesian Inference Framework to
509 Reconstruct Transmission Trees Using Epidemiological and Genetic Data. *PLoS Computational Biology*, 8(11):e1002768,
510 11 2012. doi: 10.1371/journal.pcbi.1002768.
- 511 21. Munnink, B. B., Sikkema, R. S., Nieuwenhuijse, D. F., Molenaar, R. J., Munger, E., Molenkamp, R., Van Der Spek, A.,
512 Tolsma, P., Rietveld, A., Brouwer, M., Bouwmeester-Vincken, N., Harders, F., Der Honing, R. H. V., Wegdam-Blans, M. C.,
513 Bouwstra, R. J., GeurtsvanKessel, C., Van Der Eijk, A. A., Velkers, F. C., Smit, L. A., Stegeman, A., Van Der Poel, W. H., and
514 Koopmans, M. P. Transmission of SARS-CoV-2 on mink farms between humans and mink and back to humans. *Science*,
515 371(6525):172–177, 1 2021. doi: 10.1126/science.abe5901.
- 516 22. Metreja, A., Kim, D. W., Thomson, N. R., Connor, T. R., Lee, J. H., Kariuki, S., Croucher, N. J., Choi, S. Y., Harris, S. R.,
517 Lebens, M., Niyogi, S. K., Kim, E. J., Ramamurthy, T., Chun, J., Wood, J. L. N., Clemens, J. D., Czerkinsky, C., Nair,
518 G. B., Holmgren, J., Parkhill, J., and Dougan, G. Evidence for several waves of global transmission in the seventh cholera
519 pandemic. *Nature*, 477(7365):462–465, 9 2011. doi: 10.1038/nature10392.
- 520 23. Numminen, E., Chewapreecha, C., Sirén, J., Turner, C., Turner, P., Bentley, S. D., and Corander, J. Two-phase importance

- 521 sampling for inference about transmission trees. *Proceedings of the Royal Society B: Biological Sciences*, 281(1794), 2014.
522 doi: 10.1098/rspb.2014.1324.
- 523 24. O'Toole, , Scher, E., Underwood, A., Jackson, B., Hill, V., McCrone, J. T., Colquhoun, R., Ruis, C., Abu-Dahab, K., Taylor,
524 B., Yeats, C., Du Plessis, L., Maloney, D., Medd, N., Attwood, S. W., Aanensen, D. M., Holmes, E. C., Pybus, O. G., and
525 Rambaut, A. Assignment of Epidemiological Lineages in an Emerging Pandemic Using the Pangolin Tool. *Virus Evolution*,
526 7 2021. doi: 10.1093/ve/veab064.
- 527 25. Pham, T. M., Kretzschmar, M., Bertrand, X., and Bootsma, M. Tracking *Pseudomonas aeruginosa* transmissions due to
528 environmental contamination after discharge in ICUs using mathematical models. *PLOS Computational Biology*, 15(8):
529 e1006697, 8 2019. doi: 10.1371/journal.pcbi.1006697.
- 530 26. R Core Team. R: A Language and Environment for Statistical Computing, 2022. URL <https://www.r-project.org/>.
- 531 27. Ruan, Y., Wei, C. L., Ling, A. E., Vega, V. B., Thoreau, H., Se Thoe, S. Y., Chia, J.-M., Ng, P., Chiu, K. P., Lim, L., Zhang, T.,
532 Chan, K. P., Lin Ean, L. O., Ng, M. L., Leo, S. Y., Ng, L. F., Ren, E. C., Stanton, L. W., Long, P. M., and Liu, E. T. Comparative
533 full-length genome sequence analysis of 14 SARS coronavirus isolates and common mutations associated with putative
534 origins of infection. *The Lancet*, 361(9371):1779–1785, 5 2003. doi: 10.1016/S0140-6736(03)13414-9.
- 535 28. Si, Y., de Boer, W. F., and Gong, P. Different environmental drivers of highly pathogenic avian influenza H5N1 outbreaks in
536 poultry and wild birds. *PloS one*, 8(1):e53362, 2013. doi: 10.1371/journal.pone.0053362.
- 537 29. Worby, C. J., O'Neill, P. D., Kypraios, T., Robotham, J. V., De Angelis, D., Cartwright, E. J., Peacock, S. J., and Cooper,
538 B. S. Reconstructing transmission trees for communicable diseases using densely sampled genetic data. *Annals of Applied*
539 *Statistics*, 10(1):395–417, 3 2016. doi: 10.1214/15-AOAS898.
- 540 30. Ypma, R. J., van Ballegooijen, W. M., and Wallinga, J. Relating phylogenetic trees to transmission trees of infectious disease
541 outbreaks. *Genetics*, 195(3):1055–1062, 2013. doi: 10.1534/genetics.113.154856.
- 542 31. Zhao, S., Tang, B., Musa, S. S., Ma, S., Zhang, J., Zeng, M., Yun, Q., Guo, W., Zheng, Y., Yang, Z., Peng, Z., Chong, M. K.,
543 Javanbakht, M., He, D., and Wang, M. H. Estimating the generation interval and inferring the latent period of COVID-19 from
544 the contact tracing data. *Epidemics*, 36, 2021. doi: 10.1016/j.epidem.2021.100482.

Table 1 - Summary statistics of simulated SARS-CoV-2 outbreaks in mink farms.

	Number of simulated introductions					
	1	2	5	10	20	30
Estimated number of introductions	1.2	2.1	4.5	7	12.7	14.3
Correct infectors with highest support	75%	75%	71%	74%	74%	66%
Correct infectors in 95% CI	96%	97%	96%	97%	97%	92%

545

Table 2 - Summary statistics of SARS-CoV-2 outbreak in mink farms from real data.

Parameter Inference	median (95% quantile range) of posterior
μ	$5.5 \cdot 10^{-6}$ ($4.7 \cdot 10^{-6}$; $6.4 \cdot 10^{-6}$)
m_S	11.9 (10.2; 14.1)
$r_{history}$	30.5 (17.2; 53.6)
L	1.0 (0.6; 1.5)
Tree inference	
Number of introductions	13 (11; 14)
Time of first coalescent event in history	-51.7 (-87.4; -27.9)

546

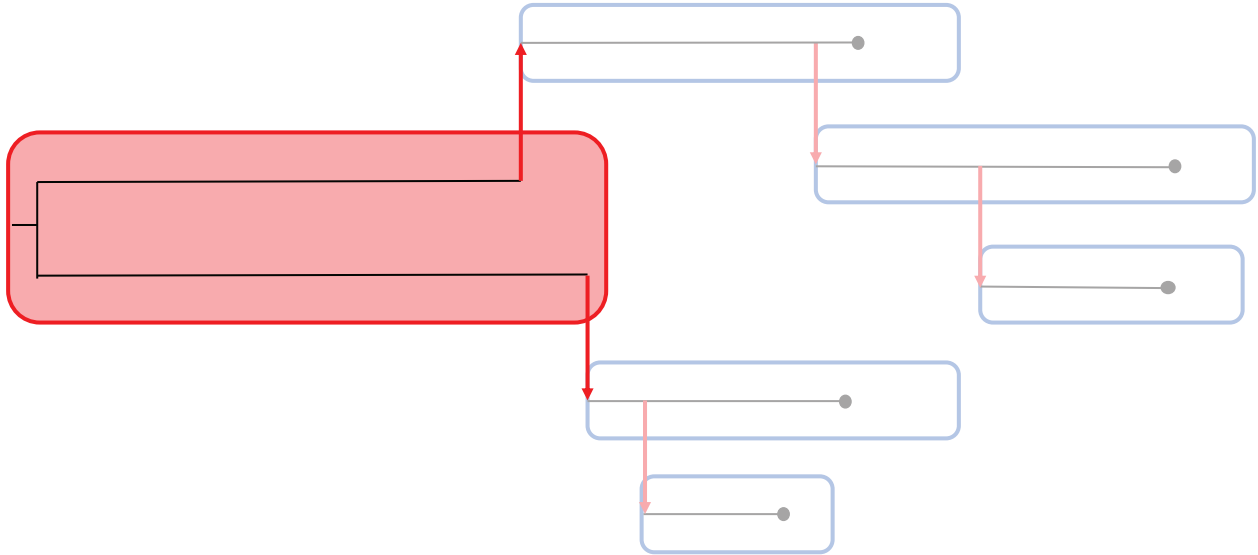
Table 3 - Prior distributions of the model parameters.

Parameter	Description	Type of distribution	Distribution parameters
$\log_{10}(\mu)$	Mutation rate	$N(\mu, \sigma)$	$\mu_{\log_{10}(\mu)} = -4; \sigma_{\log_{10}(\mu)} = 0.5$
m_G	Mean generation time interval	$D(\mu_{m_G}, \sigma_{m_G})$	$\mu_{m_G} = 1; \sigma_{m_G} = \infty$
m_S	Mean sampling time interval	$D(\mu_{m_S}, \sigma_{m_S})$	$\mu_{m_S} = 1; \sigma_{m_S} = \infty$
r	Within-host coalescent rate	$\Gamma(a_r, b_r)$	$a_r = 3; b_r = 3/1$
$r_{history}$	History host coalescent rate	$\Gamma(a_{r_{history}}, b_{r_{history}})$	$a_{r_{history}} = 1; b_{r_{history}} = 1/100$
r_{intro}	Introduction rate	$N(\mu_{r_{intro}}, \sigma_{r_{intro}})$	$\mu_{r_{intro}} = 1; \sigma_{r_{intro}} = \infty$

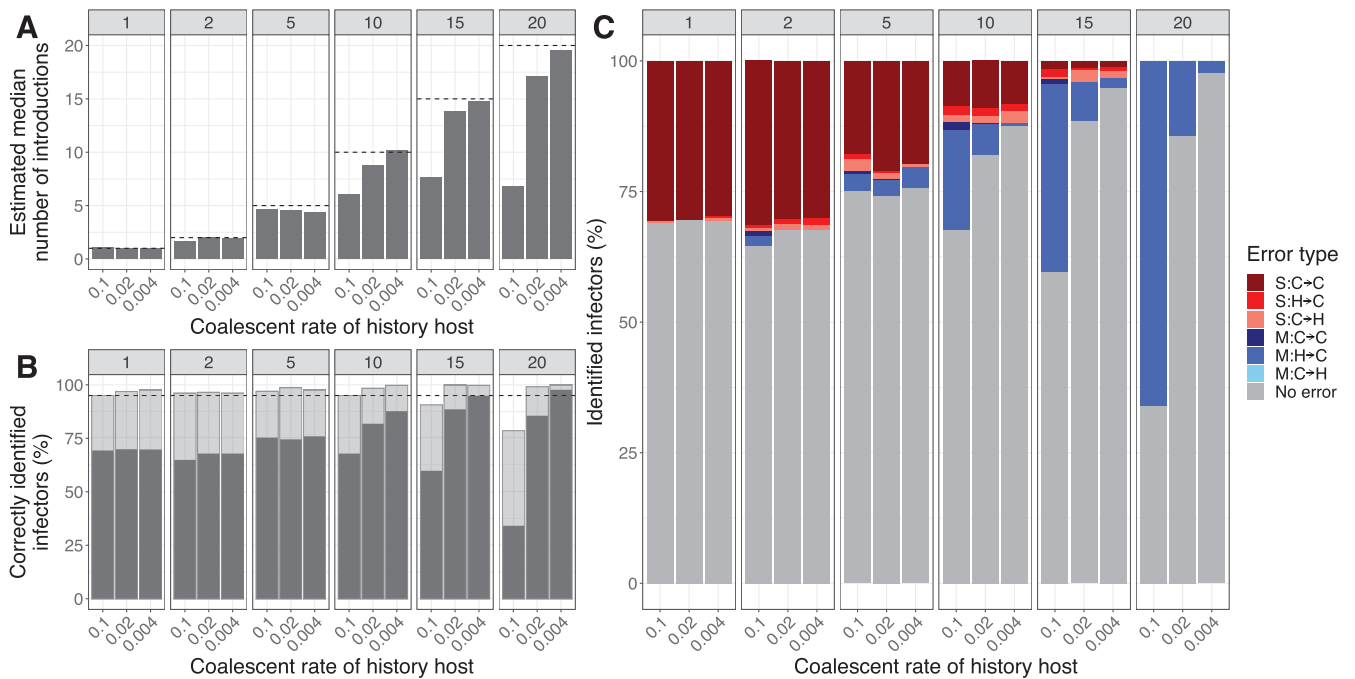
547

548 **Figure 1 - Overview of an outbreak with five sampled hosts and two introductions.**

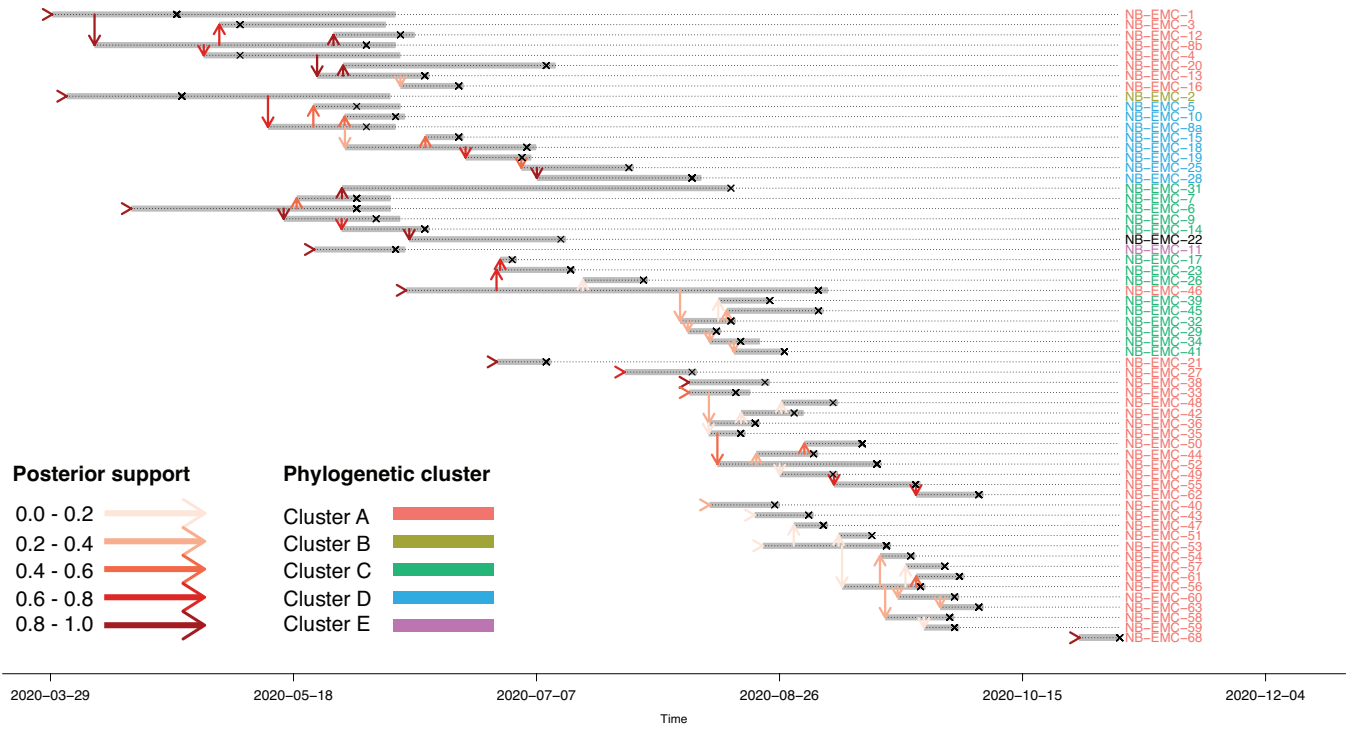
549 The index cases of the sampled hosts (blue squares) are connected via the history host (red square). Coalescence
550 of lineages happens at a different rate in the history host than in the sampled hosts. The black lines give the
551 phylogenetic tree of the outbreak and the red arrows indicate transmissions between hosts.



552 **Figure 2 - Analysis of simulated outbreaks with a varying number of introductions and coalescent rate**
 553 **($r_{history}$) in the history host.** The facets give the results for either 1, 2, 5, 10, 15, or 20 simulated introductions.
 554 **(A) The mean estimated median number of introductions.** The black line indicates the simulated number of
 555 introductions.
 556 **(B) Percentage of correctly identified infectors.** The grey bar indicates cases for which the true infector has the
 557 highest posterior weight. The transparent bar indicates cases for which the true infector is contained in the smallest
 558 set of candidate infectors with at least 95% of the posterior weight.
 559 **(C) Classification of the falsely identified infectors based on the highest support.** The grey bars indicate the
 560 correctly identified infectors. S: single transmission cluster involved, M: multiple transmission clusters involved. For
 561 the infector of a host: C2C: case becomes case, H2C: history becomes case, C2H: case becomes history.

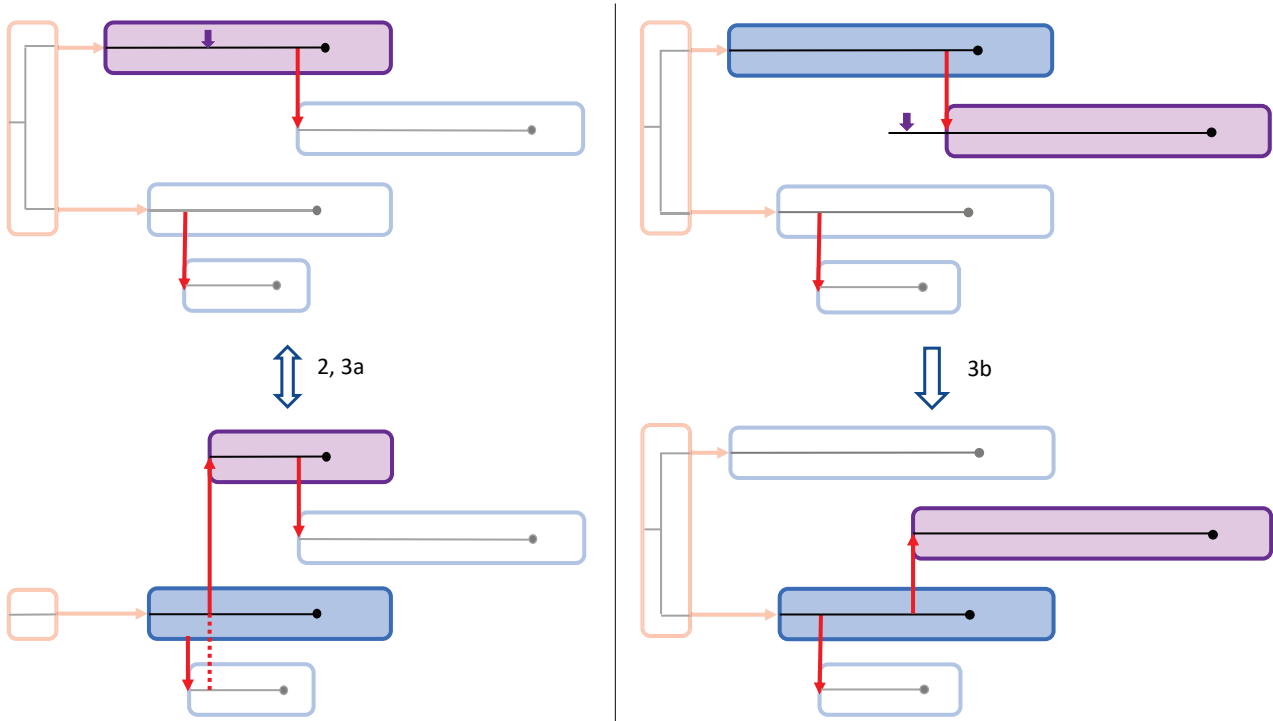


562 **Figure 3 - Maximum parent credibility transmission tree of a SARS-CoV-2 outbreak in mink farms.**
563 In total 13 introductions are found in the outbreak. Vertical arrows represent transmission links and all arrows are
564 colored according to the support in the posterior distribution. The grey bars show the infectiousness of the hosts and
565 hosts are sampled at the crosses. Host labels are colored according to phylogenetic clusters found by Lu et al. [19].



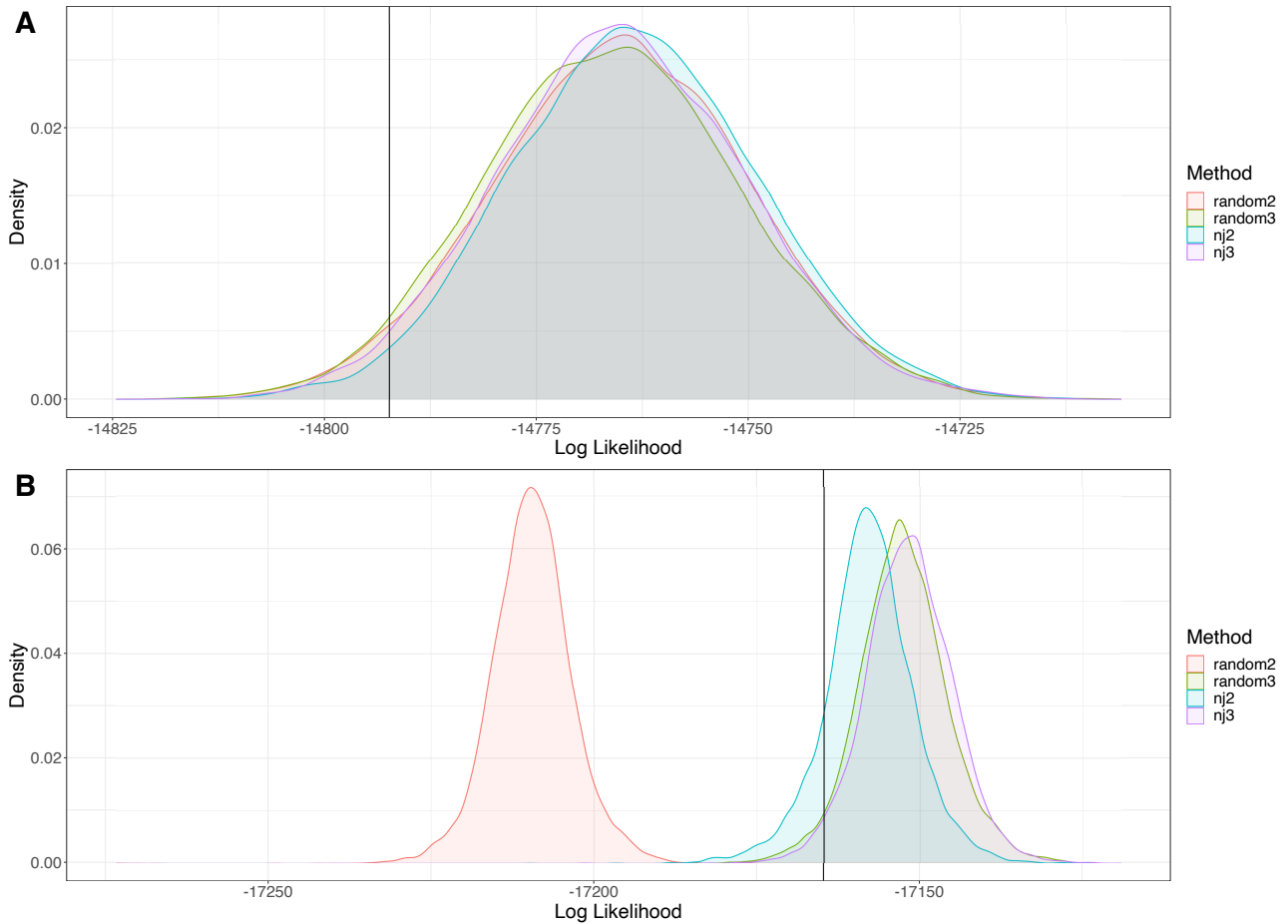
566 **Figure 4 - Proposal steps for updates between sub-trees.**

567 In purple is the focal host, with the purple arrow indicating the proposed infection time I'_i . The red arrows indicate the
568 transmission events and the history host is colored red, with the introductions as transmission from the history host.
569 2: Losing an introduction by proposing a new infector $M_i \neq 0$ for an index case. 3a: The reverse of 2, by proposing a
570 new infector $M_i = 0$ for a non-index case. 3b: Switching sub-trees by proposing a new infector $M_i \neq 0$ on a different
571 sub-tree. Situation 3b is also possible within the same sub-tree.

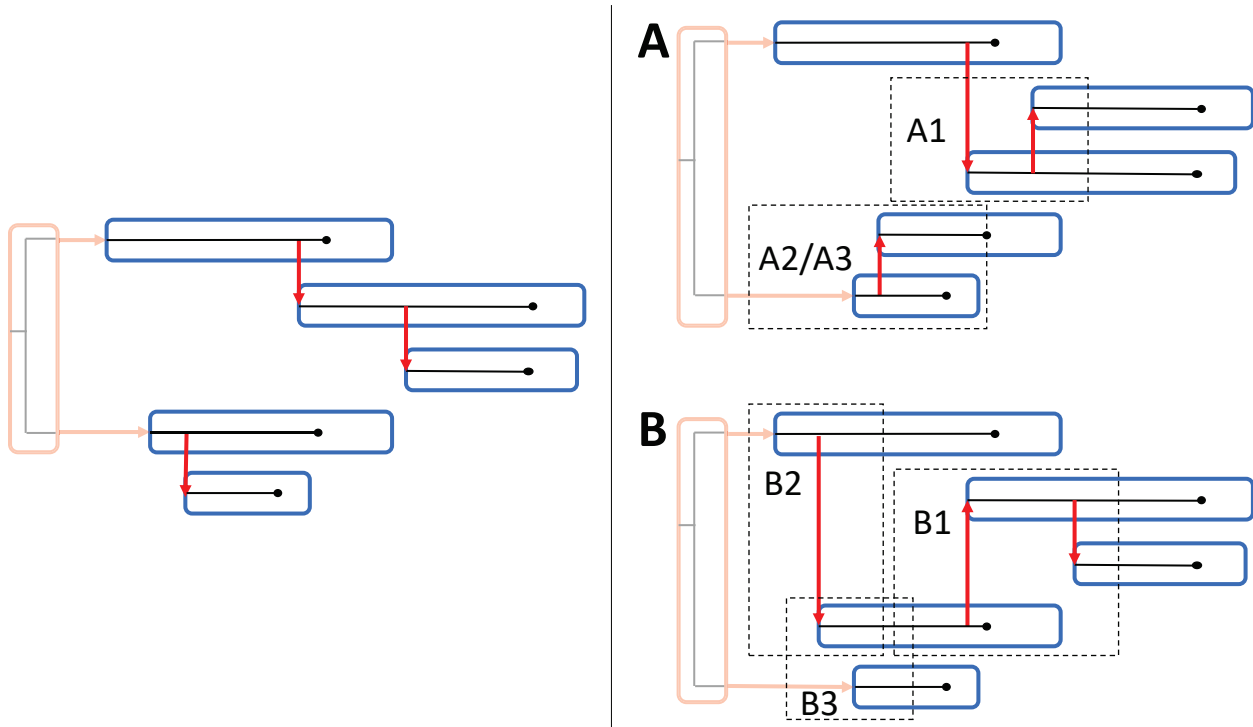


572 Supplementary Information

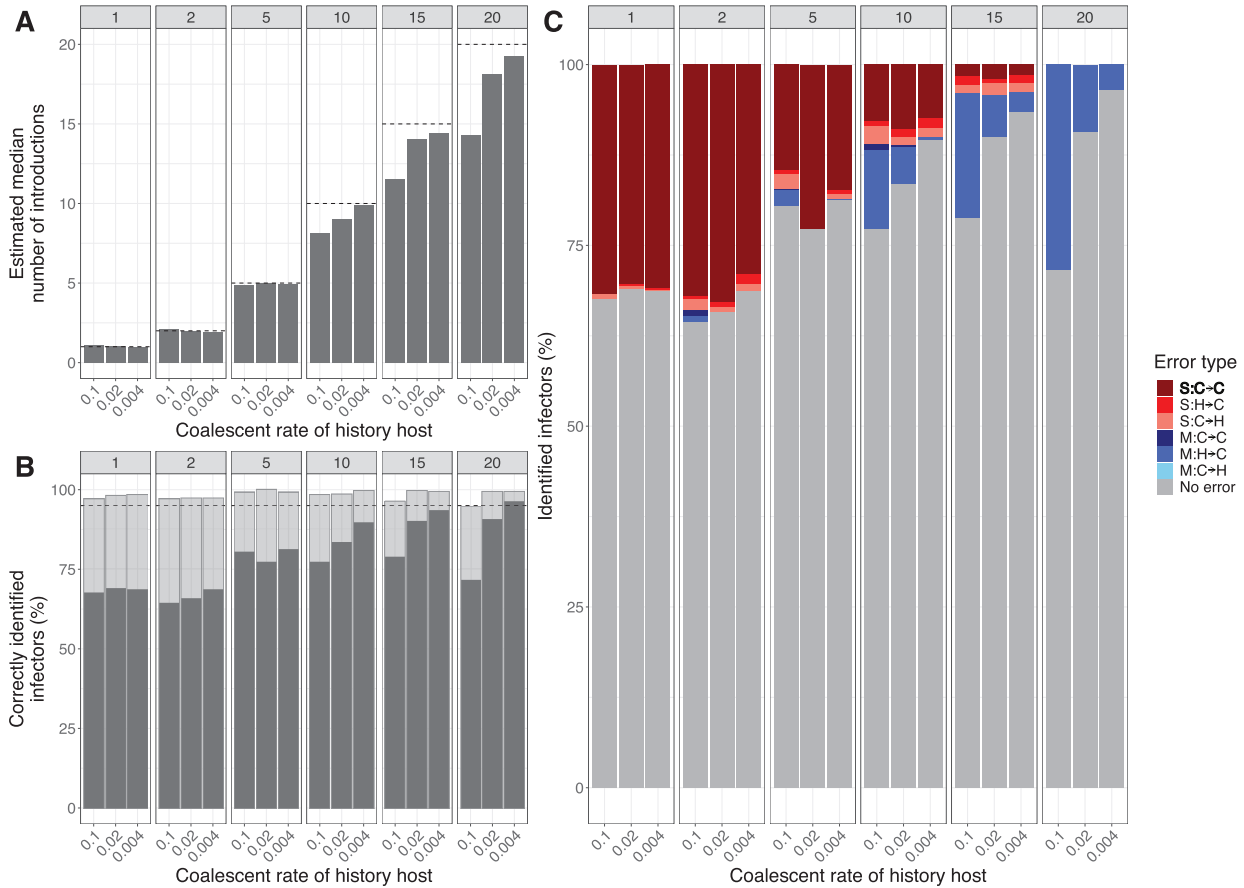
573 **Figure S1 - Comparison of MCMC and $p(\text{MC}^3)$ with and without the neighbour-joining tree initialization step.**
574 A: For low numbers of introductions (5 of the 20 hosts), there is no difference between methods in the posterior
575 log-likelihood distribution. B: Higher numbers of introductions (15 of the 20 hosts), performance of MCMC with a
576 random tree as initialization of the history host is inferior to either $p(\text{MC}^3)$, neighbour-joining tree initialization of the
577 history host or the combination of both. The latter gives the highest likelihood distribution and is chosen as default
578 option in all analyses. 'random' is random tree initialization, 'nj' is neighbour-joining tree initialization, '2' is MCMC
579 and '3' is $p(\text{MC}^3)$.



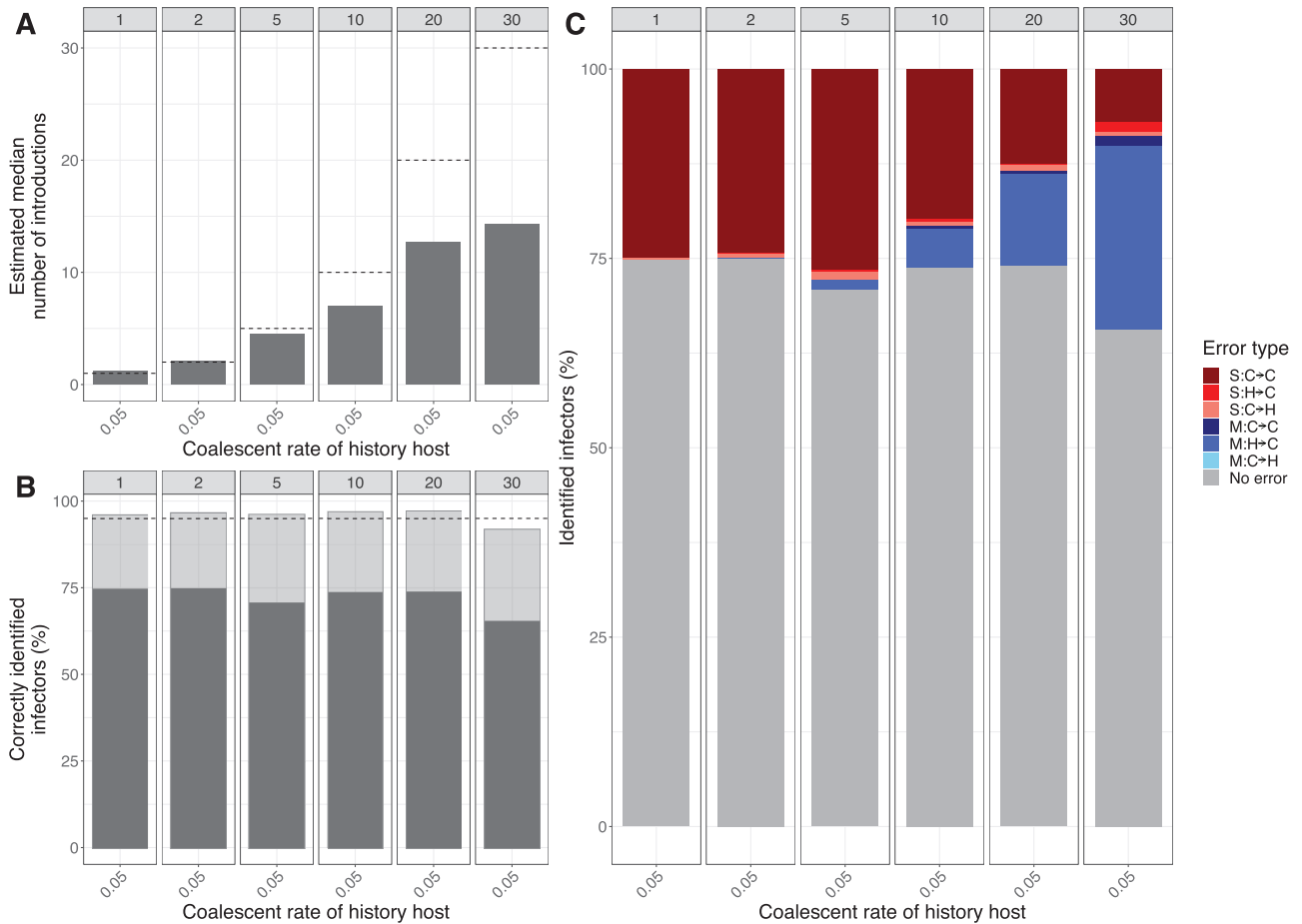
580 **Figure S2: Type of errors in the estimated transmission tree.** The left figure represents the transmission tree of
581 a simulated outbreak with 5 cases; there are 2 introductions (clusters) and 3 transmission events. The right figures
582 represents possible estimates of the transmission tree of the simulated outbreak. The vertical ordering of cases
583 in the left and the right figures is identical. The upper right figure shows errors in which an incorrect infector
584 is identified, but the incorrect infector belongs to the same cluster as the true infector (type A errors), the lower right
585 figure represents incorrect identifications of the infector in which the incorrect infector belongs to a different cluster
586 as the true infector (type B errors). In Type 1 errors neither the true infector nor the incorrect identified infector is an
587 index case. For type 2 errors, the host is an index case in the simulated outbreak but not in the estimated outbreak.
588 For type 3 errors, the host is not an index case in the simulated outbreak but is an index case in the estimated
589 outbreak.



590 **Figure S3: Analysis of simulated outbreaks with varying number of introductions and coalescent rate in the**
 591 **history host.** The model parameters are fixed at the simulation values. (A) The mean estimated median number of
 592 introductions. The black line indicates the simulated number of introductions. (B) Percentage of correctly identified
 593 infectors. The grey bar indicates cases for which the true infector has the highest posterior weight. The transparent
 594 bar indicates cases for which the true infector is contained in the smallest set of candidate infectors with at least 95%
 595 of the posterior weight. (C) Classification of the incorrectly identified infectors in the maximum credibility tree. The
 596 grey bars indicate the correctly identified infectors. S: single transmission cluster involved, M: multiple transmission
 597 clusters involved. C->C: simulated and inferred infectors are cases, H->C: simulated infector was history host,
 598 inferred infector is case, C->H: simulated infector was case, inferred infector is history host.



599 **Figure S4: Analysis of simulated outbreaks with similar parameter values as the SARS-CoV-2 outbreak in**
 600 **mink farms.** (A) The mean estimated median number of introductions. The black line indicates the simulated
 601 number of introductions. (B) Percentage of correctly identified infectors. The grey bar indicates cases for which
 602 the true infector has the highest posterior weight. The transparent bar indicates cases for which the true infector
 603 is contained in the smallest set of candidate infectors with at least 95% of the posterior weight. (C) Classification
 604 of the falsely identified infectors based on highest support. (C) Classification of the falsely identified infectors
 605 based on highest support. The grey bars indicate the correctly identified infectors. S: single transmission cluster involved, M:
 606 multiple transmission clusters involved. For the infector of a host: C->C: case becomes case, H->C: history becomes
 607 case, C->H: case becomes history.



608 **Figure S5: Maximum parent credibility transmission tree with with-host phylogenetic trees for SARS-CoV-2**
609 **outbreak in mink farms.** The farms are colored according to the clusters found by Lu et al. (2021): cluster A: red;
610 cluster B; yellow, cluster C: green; cluster D: blue, cluster E: purple, cluster unknown: black. Cluster A is divided into
611 5 smaller clusters, with cluster A1 introduced in NB-EMC-1 and cluster A2 introduced in NB-EMC-46.



612 **Figure S6: Maximum parent credibility phylogenetic tree for SARS-CoV-2 outbreak in mink farms.** The history
613 host is shown as the most-left red line, and the hosts are given in alternating colors. The black boxes represent the
614 clusters in the transmission tree, with the lowest box the assumed bigger cluster with index case NB-EMC-46.

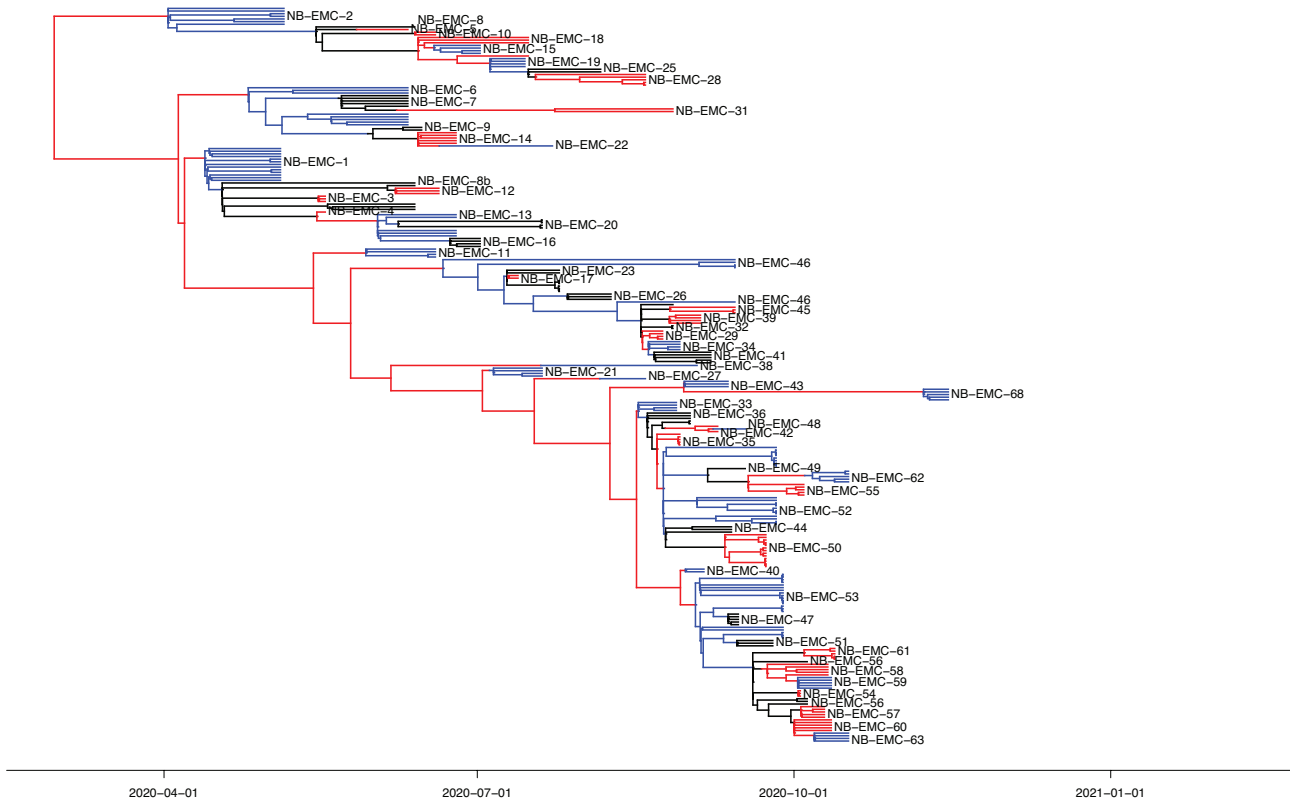
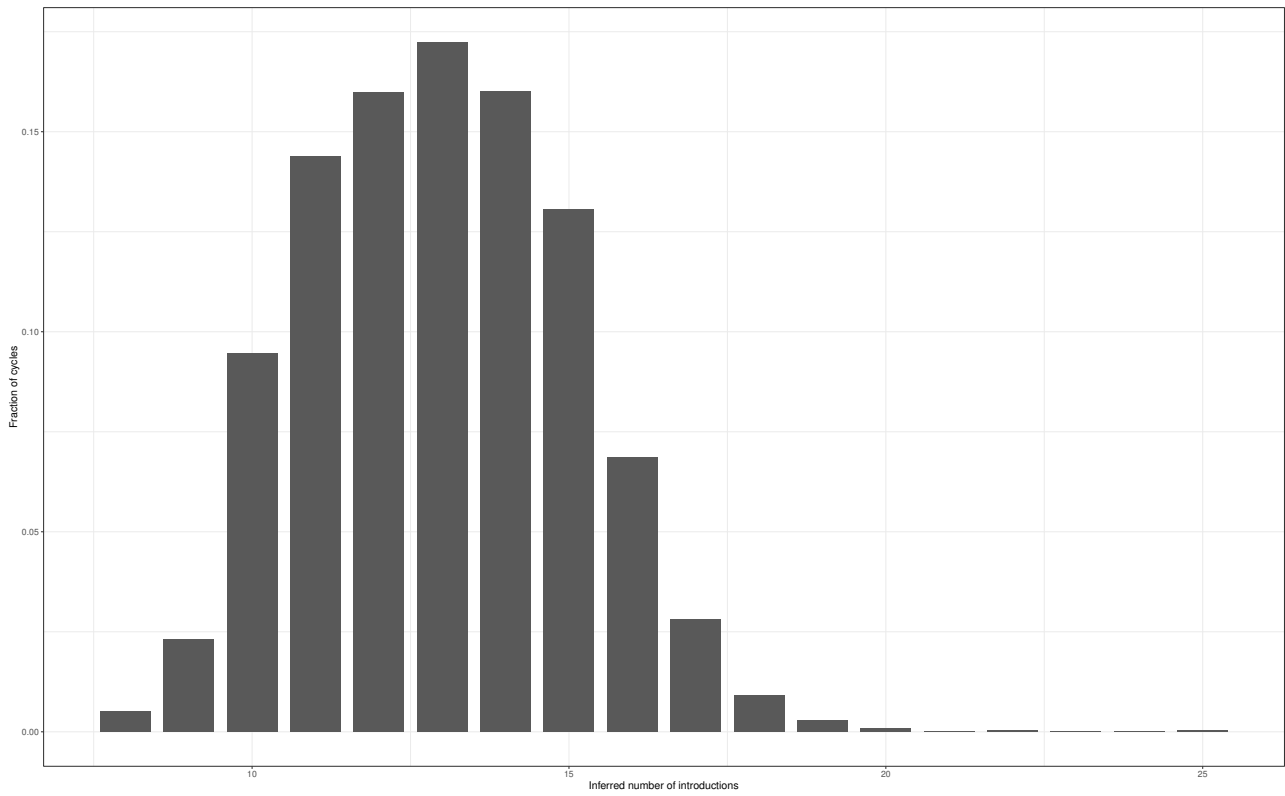
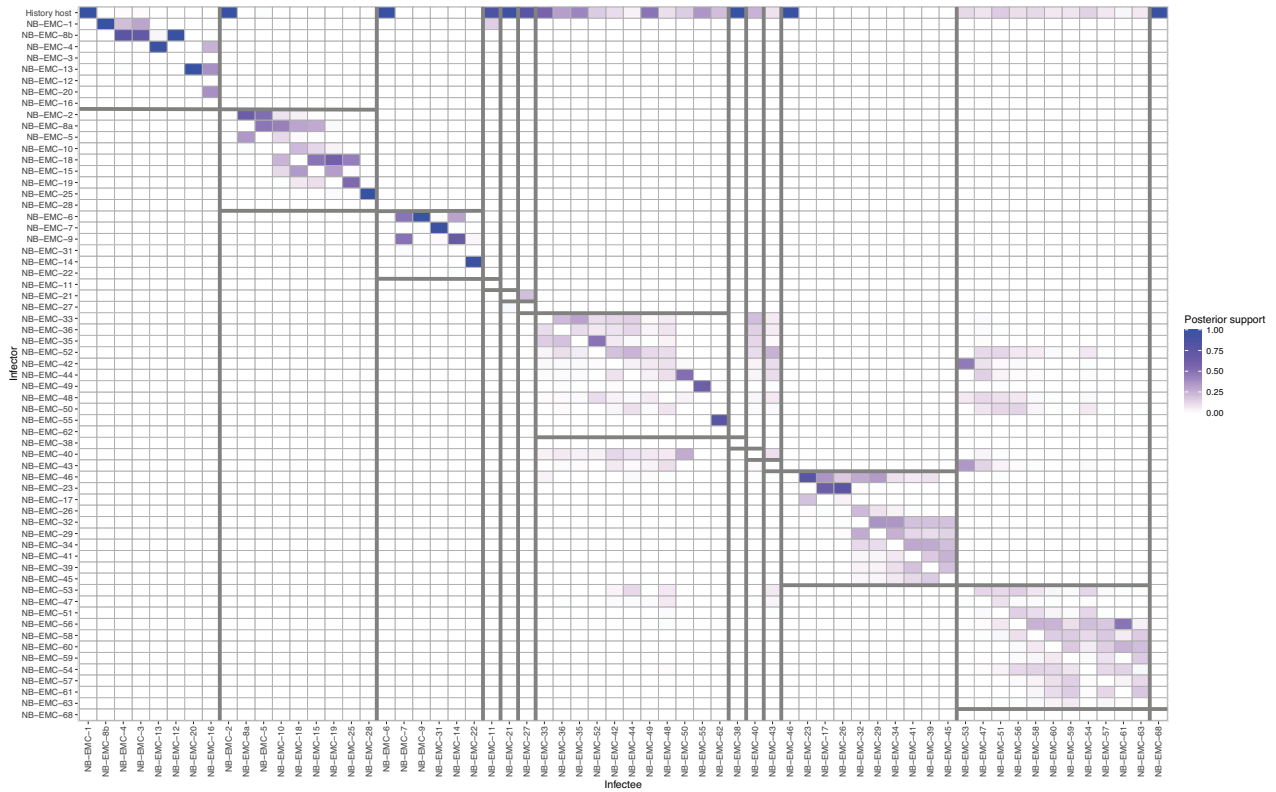


Figure S7: Histogram of number of introductions for the mink farms



615

616 **Figure S8: Posterior support of infectors of all hosts.** There is a high certainty of the index cases (infectees with the history host as infector) in the beginning of the outbreak. Transmission clusters with index cases NB-EMC-33 and NB-EMC-53 show more variation of the infectors, even outside their transmission cluster. Posterior support is shown from 0 (white) to 1 (blue). Hosts are ordered by transmission cluster and infection time. The grey bars show the transmission clusters.



621 **Table S1: Comparison between MCMC and MC³.** Differences between median posterior log-likelihood and the
 622 log-likelihood of the simulated outbreak. Results are the means from analyses of 25 outbreaks for each setting, of
 623 the 10,001st to 35,000th MCMC cycle of each outbreak analysis.

Simulated numbers of introductions	Method	Log-likelihood
4*1	MCMC random	68.3
	p(MC ³) random	70.1
	MCMC NJ	67.9
	p(MC ³) NJ	70.1
4*5	MCMC random	27.3
	p(MC ³) random	27.0
	MCMC NJ	27.5
	p(MC ³) NJ	27.0
4*10	MCMC random	9.78
	p(MC ³) random	20.0
	MCMC NJ	17.0
	p(MC ³) NJ	20.2
4*15	MCMC random	-2.04
	p(MC ³) random	14.5
	MCMC NJ	9.49
	p(MC ³) NJ	14.5

624 **Table S2: Inferring multiple introductions with varying prior information: no information, informative priors,**
 625 **and fixed parameters.** 25 outbreaks of size 20 are simulated with 5 introductions for each set of priors. The results
 626 of the model parameters are mean differences between mean estimates and the simulated value.

	No information ^c	Informative priors ^b	Fixed parameters ^a
Mean difference between estimations and simulated value			
Introductions	0.16	0.12	0.41
μ	$3.28 \cdot 10^{-5}$	$4.59 \cdot 10^{-6}$	0
m_G	0.22	0.05	0
m_S	0.40	0.02	0
r	0.08	0.10	0
$r_{history}$	15.1	4.95	0
Tree inference			
True infectors with highest support	15/20	15/20	15.7/20
True infectors in 95% CI	19.8/20	20/20	19.5/20

^a $\mu_G = 1, \sigma_G = \infty, \mu_S = 1, \sigma_S = \infty, \mu_\mu = 0, \sigma_\mu = 100$
^b $\mu_G = 1, \sigma_G = 0.1, \mu_S = 1, \sigma_S = 0.1, \mu_\mu = 10^{-4}, \sigma_\mu = 5 \cdot 10^{-5}$
^c $m_G, m_S, r = 1, r_{history} = 50, \mu = 10^{-4}$

627 **Table S3: Effective Sample Sizes of the model parameters calculated for a various number of introductions.**
 628 Results are the mean of 75 chains, i.e. 3 coalescent rates per number of introductions and 25 outbreaks per
 629 parameter set.

Simulated number of introductions	Parameters				
	μ	m_G	m_S	r	$r_{history}$
1	3565	6590	1187	512	1629
2	623	5426	907	496	1191
5	183	5399	1082	546	1314
10	411	3154	699	491	1583
15	556	1660	491	593	1479
20	373	420	227	635	1067

630 **Table S4: Effective Sample Sizes (ESS) of the model parameters for analyzing a SARS-CoV-2 outbreak in**
mink farms in the Netherlands.

Parameters	ESS
log-likelihood	633
μ	710
m, S	205
r	376
T^{history}	232

631